Modeling processes asymmetries with Laplace Moving Average.

Nicolas Raillard, Marc Prevosto, Pierre Ailliot

▶ **To cite this version:**

Nicolas Raillard, Marc Prevosto, Pierre Ailliot. Modeling processes asymmetries with Laplace Moving Average.. 2014. hal-00951767

HAL Id: hal-00951767
https://hal.science/hal-00951767

Preprint submitted on 25 Feb 2014

HAL is a multi-disciplinary open access archive for the deposit and dissemination of scientific research documents, whether they are published or not. The documents may come from teaching and research institutions in France or abroad, or from public or private research centers.

L'archive ouverte pluridisciplinaire **HAL**, est destinée au dépôt et à la diffusion de documents scientifiques de niveau recherche, publiés ou non, émanant des établissements d'enseignement et de recherche français ou étrangers, des laboratoires publics ou privés.

Modeling processes asymmetries with Laplace Moving Average.

Nicolas Raillard[a,*], Marc Prevosto[a], Pierre Ailliot[b]

[a] *Laboratoire Comportement des Structures en Mer, IFREMER, France.*
[b] *Laboratoire de Mathématiques de Bretagne Atlantique, Université de Bretagne Occidentale, Brest, France.*

Abstract

Many records in environmental science exhibit asymmetries: for example in shallow water and with variable bathymetry, the sea wave time series shows front-back asymmetries and different shapes for crests and troughs. In such situation, numerical models are available but are highly CPU-time consuming. A stochastic process aimed at modeling such asymmetries has already been proposed, the Laplace Moving Average process. The objective of this study is to propose a new estimator of the defining function in a non-parametric approach. Results based on a comprehensive numerical study will be shown in order to evaluate the performances of the proposed method.

Keywords: Laplace Moving average, Non-linear time series, FIR estimation, Splines, High-order spectrum, Asymmetries

1. Introduction

Marine coastal systems are subject to loadings due to sea waves, and long time series of the loadings are often needed to carry out a study of the performances of the system, or to assess the extreme behavior. During its lifetime, this system is likely to encounters various sea states, and thus one needs to be able to simulate long and numerous series with realistic characteristics. Many such systems are located near the shore, in shallow water and with variable bathymetry. In this context, the waves are known to be non-linear, and show high asymmetries. Two kind of asymmetries can arise in this context: the top-down (vertical) asymmetry and the front-back (horizontal) asymmetry. The former describes the different behavior of troughs compared to crests, as for waves the peaks are sharp compared to the bottom which are flatter. The latter asymmetry, referred to front-back asymmetry is linked to the time irreversibility: for example, the front steepness of crests is higher than the back one. Many other situations in environmental science or in economics data also lead to such asymmetries.

The aforementioned criterion are known to be impossible to reproduce with a Gaussian process, and models with such asymmetries must be constructed. Recently, such model has been proposed ([1, 2]), along with a description of some of its properties ([3, 4]) and an estimation procedure of some of its characteristics ([5]). But, as we will explain in the sequel, no procedure is available to retrieve the front-back asymmetries. The goal of the study is thus to propose a new method for estimating the kernel, which is an unknown function that rules the behavior of the process, and then to study the behavior of this estimator both on simulated and realistic dataset.

*Corresponding author

The paper is organized as follows: the first section introduces the model and some of its characteristics, and in particular the high-order spectrum properties that will be used in the estimation procedure, which is the aim of the second part: this section will be devoted to the introduction of the new estimator and to the comparison with the classical approach. In a third section, we will present a simulation study to assess the performances of the new estimation procedure. A comparison with a realistic dataset will also be carried out in the fourth and last section.

2. Description of the LMA model

2.1. Model construction

The construction of the process is based on a non-Gaussian noise, itself based on a non-Gaussian distribution, intended to be flexible and capable to handle heavy tails and distributional asymmetries, the *Generalized Asymmetric Laplace Distribution*:

Definition 1 (Generalized Asymmetric Laplace Distribution). *The following characteristic function defines a distribution called 'Generalized Asymmetric Laplace Distribution' ($\mathcal{GAL}$):*

$$\Phi(u) = e^{i\delta u}\left(1 - i\mu u + \frac{\sigma^2 u^2}{2}\right)^{-1/\nu},$$

where $\delta,\ \mu \in \mathbb{R}$, $\nu > 0$ and $\sigma > 0$. The cases $\nu = 1$ and $\mu = 0$ are referred to as the asymmetric Laplace distribution and the generalized symmetric Laplace, respectively.

This distribution has finite moments of any order, and more in particular, if $Y \sim \mathcal{GAL}(\delta, \mu, \sigma, \nu)$, then:

$$\begin{array}{cc} \mathbb{E}Y = \frac{\mu}{\nu} + \delta & \mathbb{V}Y = \frac{\mu^2+\sigma^2}{\nu} \\ s(Y) = \mu\sqrt{\nu}\frac{2\mu^2+3\sigma^2}{(\mu^2+\sigma^2)^{3/2}} & \kappa_e(Y) = 3\nu\left(2 - \frac{\sigma^4}{(\mu^2+\sigma^2)^2}\right) \end{array},$$

where s is the skewness and κ_e the excess kurtosis. This distribution shows great flexibly, with various shapes for the density function as it can be seen on the figure 1. This figure shows 8 densities all such that the mean is equal to 0 and variance to 1. The left plot contains symmetric distributions, while the right plot shows asymmetric densities.

Thanks to the infinite divisibility property of the $\mathcal{GAL}$ distribution, one can construct also a Levy process, with stationary and independent increments from a $\mathcal{GAL}$, called a Laplace motion (see [5]):

Definition 2 (Laplace Motion). *A Laplace motion Γ is defined by the following conditions:*

- *it starts at the origin (i.e. $\Gamma(0) = 0$);*
- *its increments are stationary and independent;*
- *the increments by the time unit ν have a centered asymmetric Laplace distribution, i.e. whose parameters are $\mu, \sigma, \delta = -\frac{\mu}{\sigma}$ and $\nu = 1$.*

This process is also referred as the Variance-Gamma process, see [6].

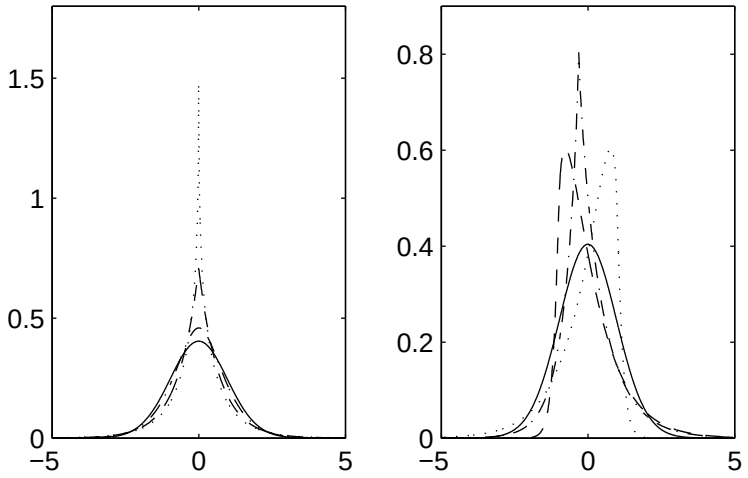

Figure 1: Densities of GAL distributions

Once we have such a process constructed, it becomes possible to define the process that will be intensively used in the sequel, namely a convolution of a Laplace motion with some function. This leads to a stationary linear process, non-Gaussian and with the ability to produce asymmetries, see [1] for more details.

Definition 3 (Laplace Moving Average). *Let* Γ *be a Laplace motion with zero mean, e.g.* $\delta = -\frac{\mu}{\nu}$*. Let also* f *be a function with values in* $\mathbb{R}$*, named* kernel *such that both* $\int_{\mathbb{R}} f$ *and* $\int_{\mathbb{R}} f^2$ *are finite. Then,*

$$X_t = \int_{\mathbb{R}} f(t-x)d\Gamma(x) \tag{1}$$

defines a stationary stochastic process on $\mathbb{R}$*, called a* Laplace Moving Average ($\mathcal{LMA}$)*. Such a process will be referred as* $\mathcal{LMA}(\mu, \sigma, \nu; f)$*.*

We thus obtain a process with three free parameters since we imposed $\delta = -\frac{\mu}{\nu}$, but which is 0 in mean. We can then add any constant to the process, so that we retrieve a four-parameters case.

2.2. Process properties

A lot a properties can be derived for this process, whose proofs can be found in the already cited articles. We will here only recall the properties that will be useful from a modeling point of view. We will describe both the marginal and the second order structure, and will also see that a same second order structure can correspond to infinitely many different processes, depending on some aspects of the kernel, namely the phase of the transfer function. Higher order structure of this process will be expressed from the kernel.

2.2.1. Marginal distribution

As it has already be seen in [1] and [2], the $\mathcal{LMA}$ process is based on $\mathcal{GAL}$ distribution, and one can compute the characteristic function of the margins for such process:

$$\phi_{X_t}(u) = e^{-iu\mu/\nu \int f} \times \exp\left\{-\frac{1}{\nu}\int_{\mathbb{R}} \log\left(1 - iu\mu f(x) + \frac{\sigma^2 u^2 f^2(x)}{2}\right) dx\right\}.$$

An interesting result is reported below:

$$\mathbb{E}X_t = 0; \tag{2}$$

$$\mathbb{V}X_t = \frac{\sigma^2 + \mu^2}{\nu} \int_{\mathbb{R}} f^2; \tag{3}$$

$$s(X_t) = \frac{\mu}{\sqrt{\nu}} \frac{2\mu^2 + 3\sigma^2}{(\mu^2 + \sigma^2)^{3/2}} \frac{\int_{\mathbb{R}} f^3}{(\int_{\mathbb{R}} f^2)^{3/2}}; \tag{4}$$

$$\kappa_e(X_t) = 3\nu \left(2 - \frac{\sigma^4}{(\mu^2 + \sigma^2)^2} \right) \frac{\int_R f^4}{(\int_{\mathbb{R}} f^2)^2}. \tag{5}$$

The scale of the kernel is still non identifiable, since any multiplicative constant on the kernel will leads to the same process, just by allowing σ and μ to change the same opposite way. So, we impose in all the sequel the constraint $\int_{\mathbb{R}} f^2 = 1$, to stay consistent with previous studies.

Another important property of this process is stated below:

Property 1. *Let X_t be a $\mathcal{LMA}(\mu, \sigma, \nu; f)$, and denote s and κ_e its skewness and excess kurtosis, respectively. Then $\kappa_e \geq 0$ and if $\kappa_e > 0$, then*

$$\frac{s(X_t)^2}{\kappa_e(X_t)} \leq \frac{2}{3} \frac{(\int f^3)^2}{\int f^4 \int f^2}. \tag{6}$$

The previous equation can be interpreted as follows: for a given skewness, the distribution can not be too light tailed (low κ_e). In every case, the tail is heavier or comparable to the one of a normal distribution, and the excess kurtosis depends on the skewness. For a Generalized Laplace distribution, the equation (6) reads $\frac{s^2}{\kappa} \leq \frac{2}{3}$ and this is the upper bound for $\frac{s^2}{\kappa_e}$ also for a $\mathcal{LMA}$, since thanks to the Cauchy-Schwarz inequality, we have for any f, $\frac{(\int f^3)^2}{\int f^4 \int f^2} \leq 1$. It means that for a $\mathcal{LMA}$, the space of values of skewness and kurtosis that can be described is smaller than for a Generalized Laplace distribution.

2.2.2. Second order structure

The usual tool for time series modeling is the second order structure, since for a Gaussian process, this structure completely defines the process. We will see that it is no more the case with $\mathcal{LMA}$ processes. For instance, the covariance function r of X_t is given by

$$r(\tau) = \frac{\sigma^2 + \mu^2}{\nu} \int_{\mathbb{R}} f(x - \tau) f(x) dx = \frac{\sigma^2 + \mu^2}{\nu} (f * \tilde{f})(\tau),$$

where $\tilde{f}(x) = f(-x)$ and $*$ is the convolution operator. The spectral density S of X_t is given by

$$S(\omega) = \frac{\sigma^2 + \mu^2}{\nu} |\mathcal{F}(f)(\omega)|^2, \tag{7}$$

where $F = \mathcal{F}(f)$ denotes the Fourier transform of f and will be referred as *transfer function* in the sequel. Those relations show that the kernel f completely determines the spectrum by the magnitude of its Fourier transform.

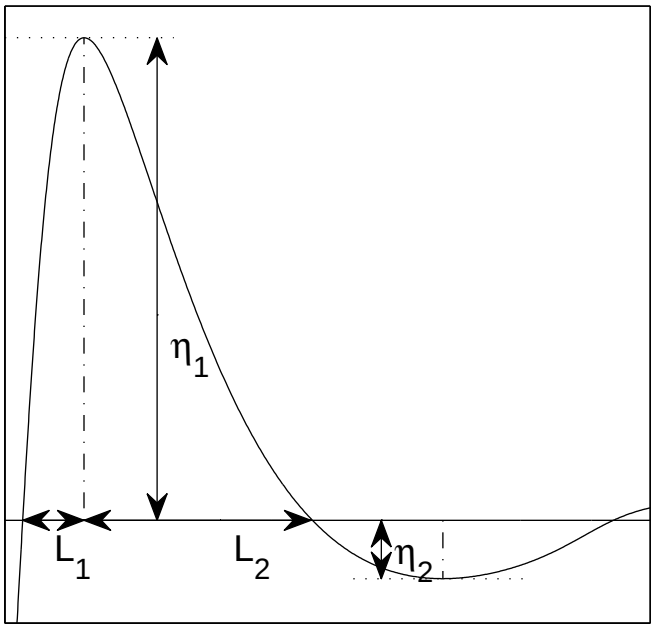

Figure 2: Asymmetry criterion

2.3. Influence of the kernel

As it can be seen from the previous equations, only the magnitude of the transfer function has an influence on the power spectrum of the process. It means that there is still infinitely many transfer functions that lead to the same covariance for the process, but that may lead to processes with different properties. We will study hereafter how the phase of the transfer function does influence the dynamical properties of the process, from an empirical point of view.

Following [7], we looked at some characteristics of the record that will help us in quantifying the asymmetries of the data. Figure 2 represents a typical wave, and the asymmetry criteria discussed hereafter:

- $\delta_{\text{up}}^{\text{Crest}} = \frac{\eta_1}{L_1}$, the crest front steepness;
- $\delta_{\text{down}}^{\text{Crest}} = \frac{\eta_1}{L_2}$, the crest back steepness;
- $\delta_{\text{up}}^{\text{Trough}}$ and $\delta_{\text{down}}^{\text{Trough}}$ can also be defined for the troughs in a similar manner.

The estimation of those characteristics from observations is straightforward, based on zero crossings of the data. A classical criterion to measure the steepness of the front face of waves is the asymmetry criterion, which is defined as the skewness of the derivative of the process, but that can be computed as the skewness of the Hilbert transform of the process (see e.g [8] and [9]).

In order to study those quantities, we simulated two $\mathcal{LMA}$ processes with the same parameters for the Laplace noise and the same second order structure, i.e same spectrum or autocorrelation function. The two kernels are depicted in the upper left plot of Figure 3. The non-symmetric kernel is $f_1(x) = x.^2 e^{-x} \mathbb{1}_{\mathbb{R}^+}(x)$ and $f_2(x) = \mathcal{F}^{-1}\left[|\mathcal{F}(f_1)|\right]$ is symmetric and has the same magnitude of its Fourier transform as f_1.

Process	$\delta_{\text{up}}^{\text{Crest}}$	$\delta_{\text{down}}^{\text{Crest}}$	$\delta_{\text{up}}^{\text{Trough}}$	$\delta_{\text{down}}^{\text{Trough}}$	A
Non-symmetric kernel	0.41	0.56	0.33	0.46	-0.21
Symmetric kernel	0.55	0.55	0.33	0.33	0.00
Gaussian process	0.45	0.45	0.45	0.45	0.00

Table 1: Estimation of the asymmetry criteria from 1000 independent replicates of process with length 2^{22} and same second order structure and same parameters for the noise: $\lambda = 0,\ \psi = 1,\ \xi = 0.2,\ \zeta = 0.6$

Examples of trajectories that can be obtained with those kernels are shown in figure 3, in the upper right plot. The trajectories seem obviously to differ although the two processes share the same autocorrelation function, as depicted in the same figure, bottom left plot.

As it can be seen from Figure 3 and Table 1, the kernel has a great influence on the tilting of the trajectories. For example, the symmetric kernel will not be able to produce any front-back asymmetries since δ_{up} and δ_{down} are equal, although the crests and troughs can behave differently. It is also noticeable that the asymmetry criterion differs clearly depending on the process. We have also seen that $\mathcal{LMA}$ processes with the same spectrum and same noise parameters will exhibit completely different behaviors. This is the reason why we will have to focus on higher order spectrum to explain such different dynamical properties. This is analogous to the marginal properties: a Gaussian distribution is described by its first two moments, but a Generalized Asymmetric Laplace will need the first four moments; a Gaussian process is characterized completely by its autocorrelation function, and a $\mathcal{LMA}$ is obviously not, according to the results above.

2.4. High-order spectrum

2.4.1. General description

To distinguish between two $\mathcal{LMA}$ with the same spectrum, we can look at the high order spectra. For sake of simplicity, we will introduce only the bispectrum, or third order spectrum, but generalization to higher order is straightforward. First of all, let us recall the expression of the third order cumulant function of any stationary stochastic process X_t:

$$C_3(\tau_1, \tau_2) = \mathbb{E}[X_t X_{t+\tau_1} X_{t+\tau_2}],$$

and by taking its Fourier transform, one obtains the third-order spectrum, also referred as bispectrum:

$$S_3(\omega_1, \omega_2) = \mathcal{F}_{2\text{D}}[C_3](\omega_1, \omega_2), \tag{8}$$

where $\mathcal{F}_{2\text{D}}$ is the 2D Fourier transform. In the sequel, the subscript will be omitted to simplify the presentation.

In next section, empirical bispectrum will be needed. Discussing the estimation of high-moments spectrum will go beyond the scope of this study, the reader may refer to [10] or [11] for a comprehensive report on this subject. We will use in the following part the estimator obtained by computing and averaging biperiodograms from overlapping blocks before a frequency-domain filter is applied. This estimates of the bispectrum S_3 will be denoted $\hat{S}_3$ in the remaining of the paper.

2.4.2. High-order statistics of a $\mathcal{LMA}$

In case of X_t being a $\mathcal{LMA}$ process with underlying Laplace noise Y_t and kernel f, one can obtain the link between its bispectrum and the kernel, following similar computations than for the

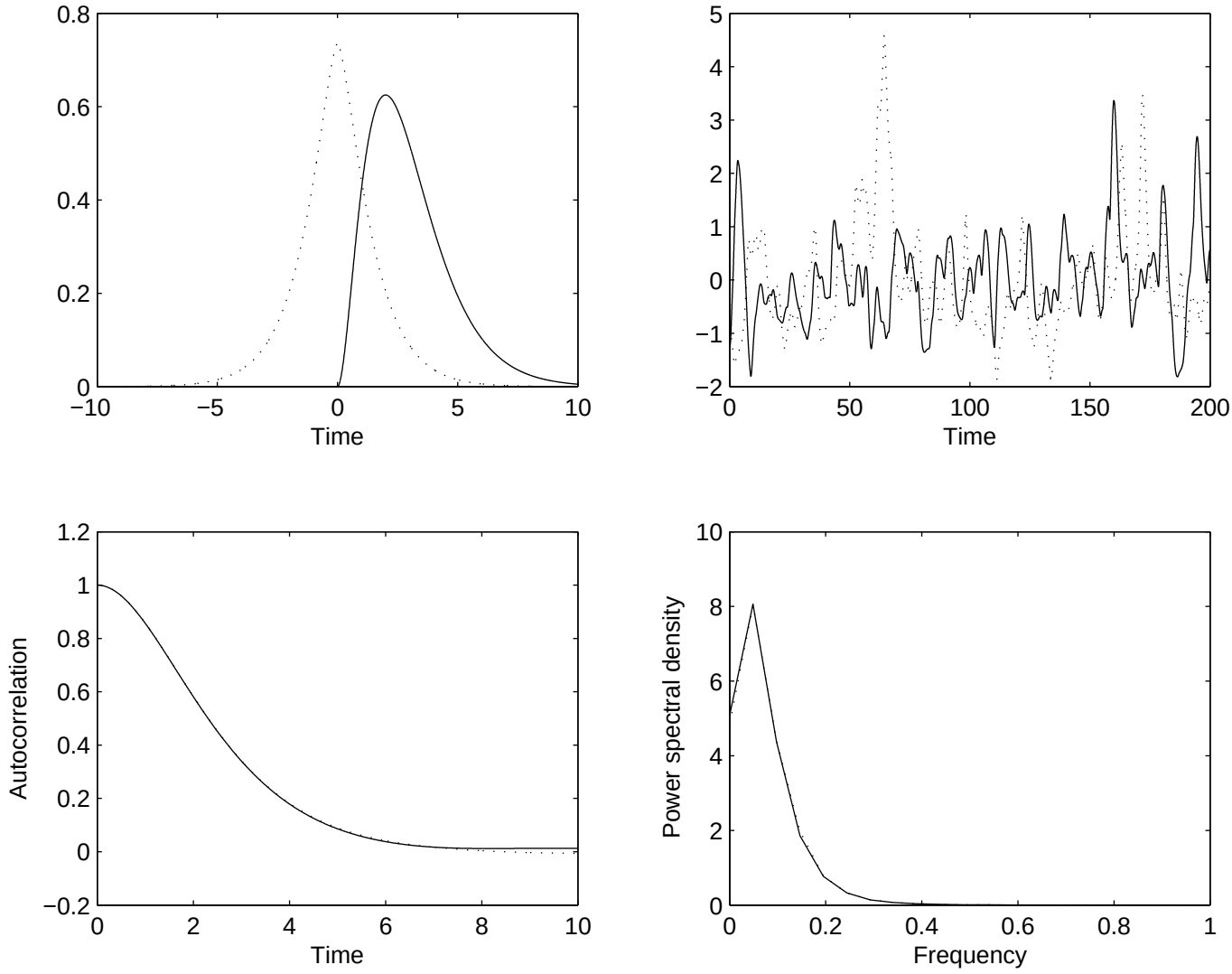

Figure 3: Example of $\mathcal{LMA}$. Top left: Kernel used; top right: Example of trajectories. Bottom left: Empirical autocorrelation function. Bottom right: Empirical power spectrum. For each plot: non-symmetric kernel f_1 in solid line and symmetric kernel case f_2 in dotted line. Parameters for the noise are $\lambda = 0,\ \psi = 1,\ \xi = 0.2,\ \zeta = 0.6$

power spectrum:

$$S_3(\omega_1, \omega_2) = s(Y_t)F(\omega_1)F(\omega_2)\overline{F(\omega_1 + \omega_2)} \tag{9}$$

where $s(Y)$ is the third order moment of the Laplace noise Y_t and $F = \mathcal{F}(f)$ the transfer function. In particular, one has the following relations between those two complex numbers:

$$|S_3(\omega_1, \omega_2)| = |s(Y)||F(\omega_1)||F(\omega_2)||F(\omega_1 + \omega_2)|, \tag{10}$$

$$\Psi(\omega_1, \omega_2) = \Phi(\omega_1) + \Phi(\omega_2) - \Phi(\omega_1 + \omega_2), \tag{11}$$

where $\Psi(\omega_1, \omega_2)$ is the angle of $S_3(\omega_1, \omega_2)$ and $\Phi(\omega)$ is the angle of $F(\omega)$.

The previous relation shows that unless the skewness of the noise is null, the kernel can be retrieved completely from the bispectrum. This will be used in the sequel to derive estimates for the kernel. The extension to the fourth-order spectrum is straightforward and allows to treat the case $s = 0$.

3. Fitting procedure

3.1. Kernel estimation

Up to now, only symmetric kernels have been estimated in the literature (see aforementioned references). However, we have seen in the previous section that a symmetric kernel is not able to retrieve front-back asymmetries existing in records. We will recall some particular cases of kernels, before introducing a new estimator.

3.1.1. Usual estimates

Assume we observe a sequence $(X_{t_1}, \ldots, X_{t_n})$ from a $\mathcal{LMA}$ with unknown parameters and kernel f. Let $\hat{S}$ be the empirical spectrum. Our goal is to a find an estimate $\hat{f}$ for the kernel that allows for asymmetries, along with respecting the second order structure of the observed process. It means that we will impose the spectrum (or autocorrelation) to be the same as the observed one. Thus the kernel (or finite impulse response), will have the square magnitude of its Fourier transform held fixed to the observed spectrum, i.e. $|\mathcal{F}\hat{f}|^2 = \hat{S}$. From the previous relation, it is clear that we still have an infinite number of kernel with the same magnitude, allowing only the phase to change, and we take estimates $\hat{f}$ of the kernel f as following:

$$\mathcal{F}\{\hat{f}\}(\omega) = \sqrt{\hat{S}(\omega)}\exp\{i\hat{\Phi}(\omega)\}, \tag{12}$$

where $\hat{\Phi}$ is an unknown function, that has to be estimated. Three classical kernels in signal processing are detailed bellow:

Symmetric kernel. This is the kernel used in reference studies. It is obtained by assuming $\hat{\Phi} = 0$. This is a non-causal kernel, symmetric with respect to the origin, but that cannot be adequate for modeling front-back asymmetries;

Anti-symmetric kernel. Assume the phase is $\hat{\Phi}(\omega) = -\operatorname{sgn}(\omega)\frac{\pi}{2}$. Then the kernel will be odd. It can be seen from eq. (6) that the resulting process will have a skewness of 0, and thus can not model marginal asymmetries. Moreover, it is shown in [12] that a $\mathcal{LMA}$ with an odd kernel can not disclose any irreversibility, and we thus decided to drop this model in the sequel.

Minimum Phase kernel. The particular case of minimum phase kernel is obtained by setting $\hat{\Phi} = \mathcal{H}\{\log\sqrt{\hat{S}}\}$, i.e. we have a direct relation between the magnitude and the phase via the Hilbert transform $\mathcal{H}$. This kernel is causal (null for negative lags), thus asymmetric, and allows for front-back asymmetries. This is the estimate obtained when fitting a stationary ARMA model, in a discrete-time context.

3.1.2. Spline estimator for the phase

None of the kernels presented above may be suited for the observed series, because all of them rely on a strong assumption on the process that cannot be verified easily. In order to adjust the kernel to the records, a classical approach is to use the *Bicepstral method*. In this method, a kernel estimate is obtained by the complex cepstrum, as described in [13, 10]. This method relies on 2D Fourier transform to identify an arbitrary kernel, by inverting the relation 9. this method will be used as a reference. Instead of this method, we propose here to estimate the phase of the transfer function with smoothing splines. Splines are piecewise polynomials smooth functions. They are defined by their knots, their degree, and the coefficients of the polynomials within each knot (see e.g. [14] and references therein for more details). The vector of coefficients will be denoted θ in the sequel.

We used this tool to estimate the phase Φ, by approximating this unknown function by a cubic spline function, $\Phi_s(\omega;\theta)$. The estimation of the coefficients of the smoothing spline can be performed by using the relation (11). $\hat{\theta}$ is defined by

$$\hat{\theta} = \arg\min_{\theta} \sum_{i,j} |\hat{S}_3(\omega_i,\omega_j)|(1-\cos\left(\hat{\Psi}(\omega_i,\omega_j) - \Phi_s(\omega_i;\theta) - \Phi_s(\omega_j;\theta) + \Phi_s(\omega_i+\omega_j;\theta)\right), \qquad (13)$$

where the distance $1-\cos(.)$ was used because the phase is unchanged when adding $2k\pi$ for any $k \in \mathbb{Z}$. The weights $\hat{S}_3(\omega_i,\omega_j)$ are added because the angle is badly estimated for very small values of the magnitude, and thus we reduce the importance of such observations. We used a numerical optimization algorithm to solve this problem. This method will be refered as the 'Spline method' in the sequel.

3.2. Parameters estimation

In this section we will assume the kernel to be known. The aim is to find estimates for the four parameters of the underlying Laplace noise. Following [5], we will use a moment estimator based on the marginal moments, expressed earlier (equations 2—5), meaning that we will replace the moments values in those equations by their empirical counterparts, and inverting the obtained system.

As described in [5] it can happen that this system has no solution, because the constraint in equation (6) may not be fulfilled by the empirical estimates of moments, due to the sample variability of these quantities or because the marginal distribution is not a $\mathcal{GAL}$. In this case, an approximate solution is chosen, and one can refer to [5] for the choice of the approximation. We will follow their choice in this study.

The consistency of the estimates can be derived from the strong mixing property of moving averages with respect to Lévy measures, as $\mathcal{LMA}$ are (see, for example [15]). This ensures that the empirical moments converge to the true values, leading to consistency.

A numerical study of the performances of these estimates can be found in Section 4.

True process	Minimum phase kernel							
Parameter	ξ	ζ	L^2 error	A	$\delta_{\text{up}}^{\text{Crest}}$	$\delta_{\text{down}}^{\text{Crest}}$	$\delta_{\text{up}}^{\text{Trough}}$	$\delta_{\text{down}}^{\text{Trough}}$
Actual values	0.2	0.6	NA	-0.21	0.41	0.56	0.33	0.46
True Kernel	0.25 (0.08)	0.55 (0.12)	NA	-0.21 (0.07)	0.41 (0.01)	0.56 (0.03)	0.33 (0.01)	0.47 (0.03)
Symmetric kernel	0.25 (0.08)	0.55 (0.12)	0.50 (2.10)	0.00 (0.06)	0.57 (0.02)	0.57 (0.02)	0.34 (0.01)	0.34 (0.01)
Minimum phase kernel	0.25 (0.09)	0.56 (0.12)	0.00 (0.01)	-0.21 (0.07)	0.42 (0.01)	0.56 (0.02)	0.35 (0.01)	0.49 (0.02)
Bicepstral method	0.19 (0.06)	0.42 (0.09)	0.17 (1.12)	-0.33 (0.16)	0.89 (0.17)	3.02 (0.40)	0.69 (0.07)	1.30 (0.41)
Spline kernel	0.25 (0.08)	0.54 (0.12)	0.01 (0.03)	-0.16 (0.09)	0.44 (0.02)	0.57 (0.02)	0.33 (0.01)	0.42 (0.02)
True process	Symmetric kernel							
Parameter	ξ	ζ	L^2 error	A	$\delta_{\text{up}}^{\text{Crest}}$	$\delta_{\text{down}}^{\text{Crest}}$	$\delta_{\text{up}}^{\text{Trough}}$	$\delta_{\text{down}}^{\text{Trough}}$
Actual values	0.2	0.6	NA	0.00	0.55	0.55	0.33	0.33
True Kernel	0.23 (0.07)	0.56 (0.10)	NA	0.00 (0.07)	0.55 (0.02)	0.55 (0.02)	0.33 (0.01)	0.33 (0.01)
Symmetric kernel	0.24 (0.07)	0.56 (0.10)	0.00 (0.00)	0.00 (0.07)	0.57 (0.02)	0.57 (0.02)	0.33 (0.01)	0.33 (0.01)
Minimum phase kernel	0.24 (0.07)	0.63 (0.10)	0.48 (2.00)	-0.16 (0.08)	0.42 (0.01)	0.57 (0.03)	0.34 (0.01)	0.49 (0.02)
Bicepstral method	0.16 (0.05)	0.43 (0.08)	0.25 (1.38)	-0.26 (0.10)	1.08 (0.09)	3.49 (0.33)	0.82 (0.08)	1.34 (0.37)
Spline kernel	0.24 (0.07)	0.56 (0.10)	0.01 (0.01)	0.01 (0.08)	0.55 (0.02)	0.55 (0.02)	0.33 (0.01)	0.33 (0.01)

Table 2: Parameters estimation for two process types and different models for the kernel. In bracket, the standard deviation based on 1000 i.i.d replications.

4. Simulation results

We will study the results for two different kernels: a minimum phase kernel and a symmetric kernel, both leading to the same second order structure. Those kernels can be seen in the figure 3, on the upper-left plot.

In this section, the kernel is known, and we compared the four estimation of the kernel. The procedure is the following, repeated 1000 times:

1. Simulate a $\mathcal{LMA}$ with known kernel (symmetric and minimum phase);
2. Fit the models to the simulated process, which give an estimate for the kernel and for the parameters;
3. Simulate the fitted model to compute the dynamical characteristics on a long realisation.

Results can be found in the table 2 for the estimates of the marginal parameters in the first two columns, while the five others contains information about the dynamical behavior of the fitted process for each model.

As is can be seen from this table, the tree estimated kernels (Symmetric, Minimum phase and Spline) leads to similar results both in terms of bias and variance. There is systematic positive bias in estimating ξ while the parameter ζ is under-estimated. This may be due to the correlation between those two estimates (not shown here). The Bicepstral method for estimating the kernel leads to rather different results, with a lower variance, but a higher bias for both parameters. This is due to its bad estimation of the kernel, as it can be seen in the third column of Table 2, which contains the L^2 distance between the true kernel and the estimated one: $\int (f(x) - \hat{f}(x))^2 dx$. We found that using the wrong model leads to a bad estimation for the kernel, with substantial bias. It is then interesting to observe that the Spline model provides a good estimate in both cases, almost as good as the right model, with a slightly higher variance. When comparing to the kernel obtained by the Bicepstral method, we see a great improvement. Due the bad estimation of the kernel for this method, the system of equation (2—5) has more often no solution than with the other method (4.5% for this method, less than 1% for the others), which explains the higher bias in the estimates of the marginal parameters. We also studied numerically the importance of the number of knots of the splines and their location, but found that those two parameters do not have a great influence on the results, so results will be omitted for sake of conciseness.

Figures 4 and 5 allow to compare the kernel estimates for the two cases of Minimum phase kernel and Symmetric kernel. From these plots, it is clear that the spline model allows to recover the asymmetries in the kernel, by allowing the phase to be non-zero in the minimum phase case (right bottom plot, Figure 4), while for the symmetric kernel case, the obtained kernel is almost symmetric (right bottom plot, Figure 5). This is important in practical applications, since it might be interesting to recover the asymmetries in the records.

As stated in Section 2, one needs additional criteria than the parameters of the Laplace noise to fully describe the ability for the fitted process to recover the characteristics of the original data. Hence, we compared the dynamical properties introduced earlier. Results are given in the four rightmost collumns of Table 2. It can be concluded from this table that the spline model allows to retrieve the shape of the 'waves' for the two type of processes considered here. This was not possible neither by the use of the symmetrical kernel nor the minimum phase kernel. We also found that the biceptrum method was not well suited, since the estimated valued differs greatly from the true values. This is the reason why we did not use this estimator in the application part that follows.

5. Application to wave times series

5.1. Data description

In this section, the method to fit a $\mathcal{LMA}$ process will be carried out on a time series of sea wave measured in a wave flume on a varying bottom, in the situation described in Figure 1 of [16]. The wave flume is forced from the left with infinite-depth Gaussian waves, with a typical JONSWAP spectrum with $\gamma = 3.3$ (see e.g [17] Eq. 2.4.1), and waves propagate to the right and tends to shoal as the depth decrease. At a fixed location (point 8, situated at $X = 7m$, following the notations in [16]), one obtains a time series of elevation of the free surface, presented in the upper-left corner of figure 7. It can be seen from this plot that the data indeed exhibits differences between front and back slopes, revealing time-irreversibility (see the values in Table 3), and also discrepancies between crests and troughs (vertical asymmetry, refer to the positive value of the skewness). Figure 6 represents the power density spectrum, obtained by the periodogram. In this plot, we see three

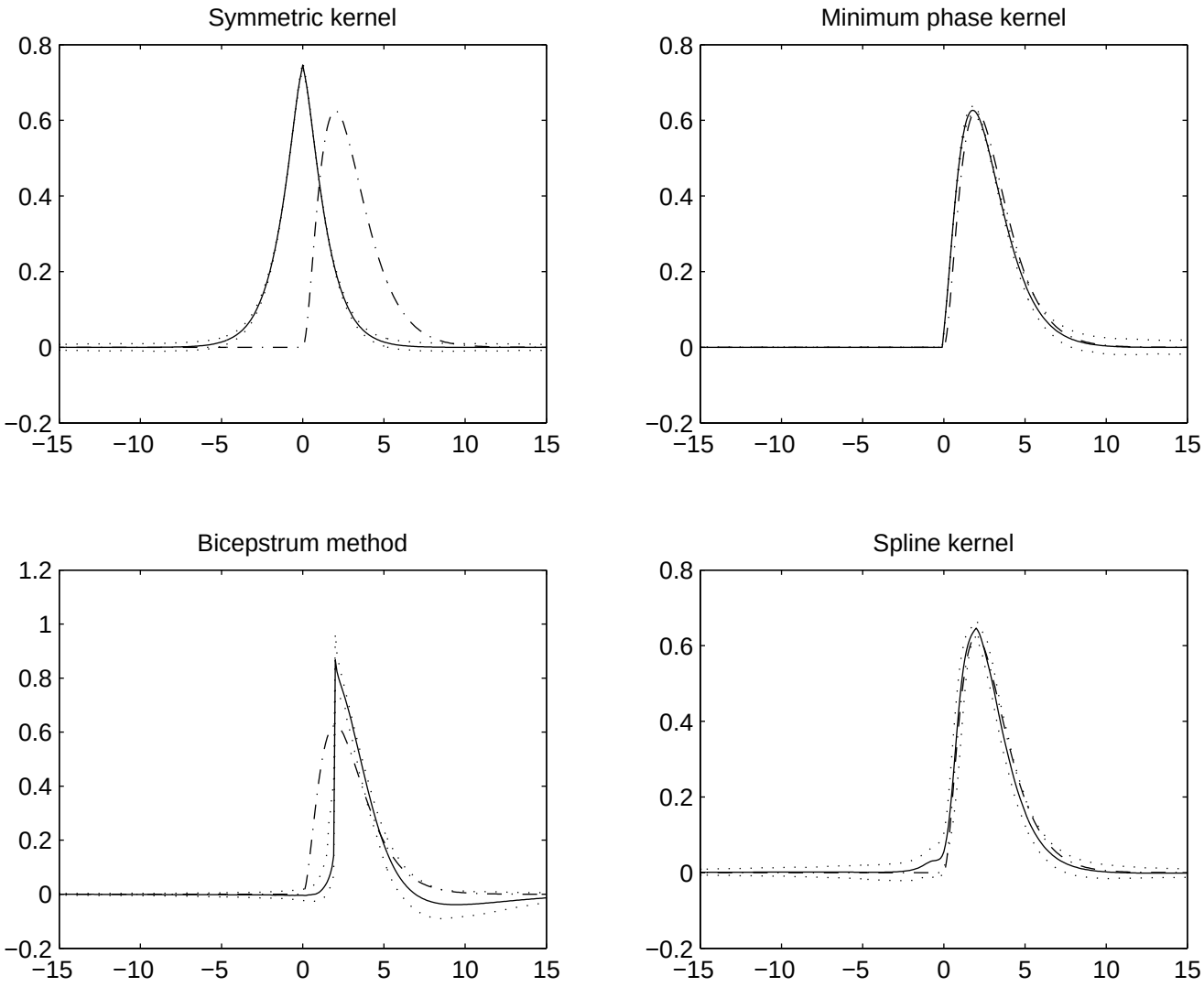

Figure 4: Estimation of the kernel for a minimum-phase process and three different estimates for the kernel. Dashed-dotted line: true kernel; solid line: mean estimated kernel; dotted line: 95% confidence interval based on 1000 i.i.d. replications.

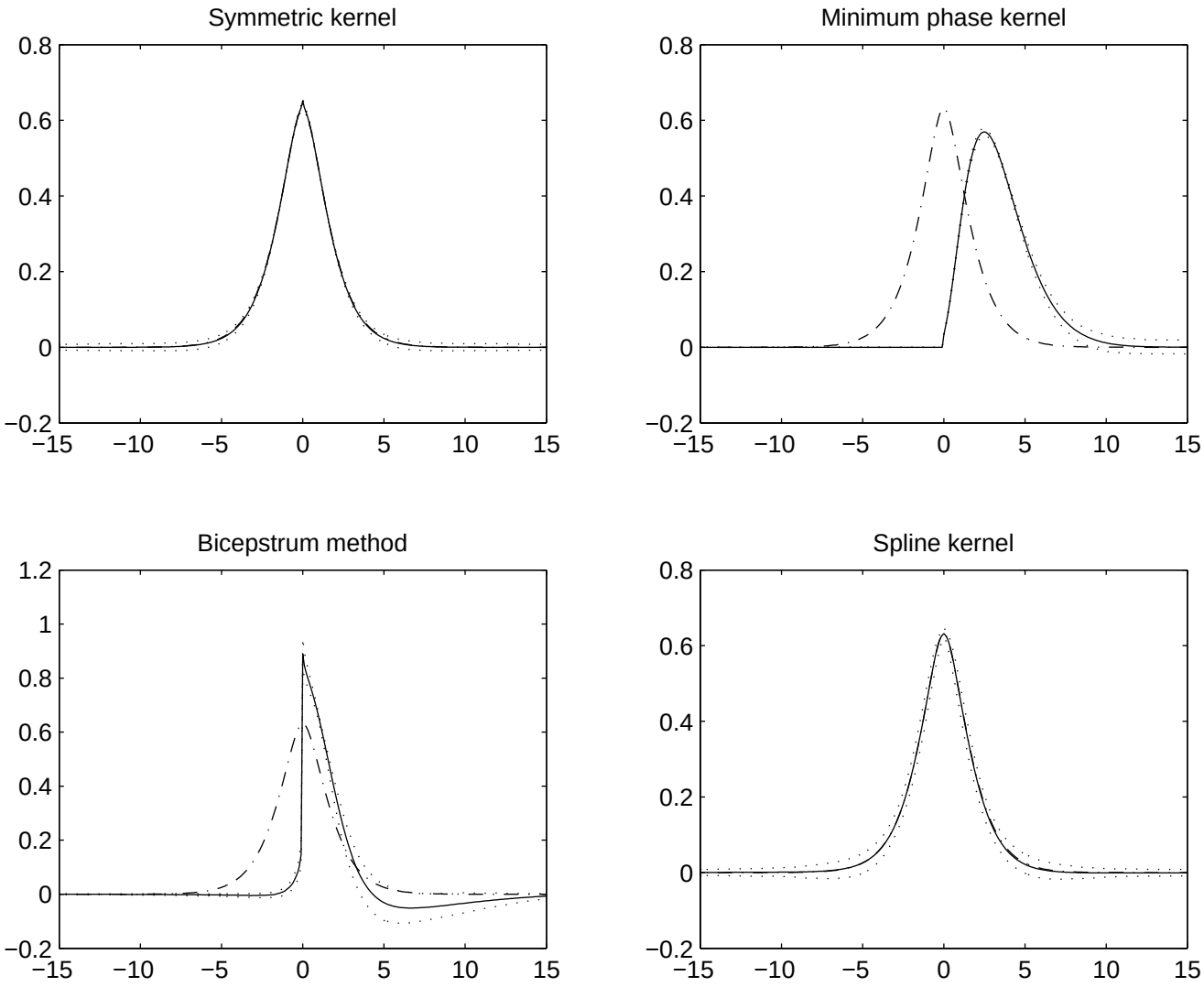

Figure 5: Estimation of the kernel for a symmetric process and three different estimates for the kernel. Dashed-dotted line: true kernel; solid line: mean estimated kernel; dotted line: 95% confidence interval based on 1000 i.i.d. replications.

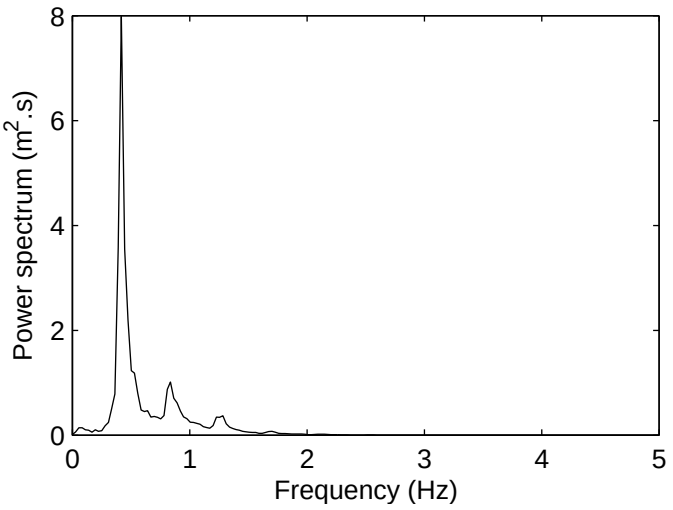

Figure 6: Power spectral density of observations.

main peaks which appear due to non-linear interactions between waves, because only a unimodal power density spectrum was introduced in the wave flume. Thoses non-linear interactions are more clear when looking at the bisepctrum, in which one can see the peaks at coupled frequencies. We recall that for a Gaussian process, the bispectrum will be identically zero, so such a model will not be suited here.

In fact, the marginal distribution is too lightly tailed compared to a $\mathcal{GAL}$ distribution (see eq. 6). To go through this problem, we transformed the process so that its marginal distribution lie in the acceptable space for a $\mathcal{GAL}$ distribution, which is a quite usual way in time series modeling with box-cox transforms. In the upper-left corner of Figures 7 to 9 and in the first line of Table 3, one can find descriptive statistics of this process.

The fitting procedure is then the following, for each model:

1. Transform the original data X with the non-linear transform $Y = sign(X)e^{abs(X).^{1-sign(X)/2})-1}$;
2. Fit each model to the transform data Y;
3. Simulate the fitted model on a very long sequence;
4. Validate marginal distribution, second and third-order structures;
5. Estimate the dynamical properties aforementioned on the process transformed back to the original scale;
6. Estimate the variability with parametric bootstrap (see e.g [18]).

All the results that follows concerns the processes in the original scale, not on the transformed scale, except for the kernel.

5.2. Analysis of the fitted $\mathcal{LMA}$

Three kernels already used in Section 4 will also be used here, namely the symmetric kernel, the minimum phase kernel and the spline kernel. Those three fitted models will then be compared. Because no usual criterion for model selection such as BIC is available for the present study, we will focus on other properties of the processes, introduced earlier. First, we will study the margins

Parameter	Median	Skewness	Kurtosis	Asymmetry	$\delta_{\text{up}}^{\text{Crest}}$	$\delta_{\text{down}}^{\text{Crest}}$	$\delta_{\text{up}}^{\text{Trough}}$	$\delta_{\text{down}}^{\text{Trough}}$
Observations	-0.10	0.89	4.87	-0.63	3.88	5.29	2.03	2.82
Symmetric kernel	-0.15	1.08	5.29	0.00	5.10	5.12	3.07	3.08
	(0.04)	(0.10)	(0.65)	(0.01)	(0.28)	(0.29)	(0.16)	(0.16)
Minimum phase kernel	-0.11	1.04	5.25	0.37	4.42	4.90	3.44	2.81
	(0.04)	(0.10)	(0.80)	(0.07)	(0.24)	(0.39)	(0.17)	(0.20)
Spline estimated kernel	-0.10	0.97	5.07	-0.32	4.37	5.70	2.99	3.07
	(0.03)	(0.08)	(0.62)	(0.04)	(0.34)	(0.31)	(0.16)	(0.12)

Table 3: Dynamical criterion estimates for the three models. In brackets, the standard deviation obtained via parametric bootstrap.

and the second and third order dependence structure of the fitted models, before looking at the dynamical properties.

The kernels corresponding to each model are given in Figure 8. One can clearly see the differences between the kernels, in particular the spline estimated kernel, which is neither symmetric nor minimum phase. It can be seen from theses plots that the kernels look almost like a typical wave. However, as stated before, kernels are difficult to interpret and one has to look at different criteria. We checked that both the marginal distribution and the second order structure of the original process are respected by the three fitted models. It is also interesting to look at trajectories, although it can only give an idea of the features, that should be quantified. Such trajectories are depicted in Figure 7.

To study more deeply the differences between the three fitted models, we looked first at the bispectrum, in order to see if one can retrieve the coupling between components, symbolized by the non-zero values of the bisepctrum. The logarithm of the absolute value of each bispectrum is reported in Figure 9, the angle of each bispectrum can be found in Figure 10. Figure 9 shows that globally, the shape of the bispectrum is well retrieved, much better than with a Gaussian process for which the bispectrum would be identically zero. However, we observe more low-frequency peaks on the bispectra of fitted models, and less peaks at high frequencies, and this is in fact due to the constraint imposed by a linear process via relation 11. From figure 10 is seems the kernel whose phase is estimated thanks to splines appear to outperforms the other models and that the shape of the phase of the bispectrum is well retrieved, and in particular it allows to recover the phase with less noise that from the observations. As expected, the symmetric kernel has a zero phase, and the phase of the minimum phase model is rather complicated, but linked to the Hilbert transform of the spectral density of the process, and both of these are far from the observations.

To conclude on this analysis, we found out that the fitted Spline model allows to retrieve the fourth four moments of the process, the second order dependance structure and some characteristics of the bispectrum, much better than with the classical method. We will now look at the tilting properties of the models, and compare them to the observed data, in the original scale, meaning that the fitted models are transformed back via the inverse of the marginal transform.

As it can be seen from Table 3, the Spline model globally outperforms the two other models as far as dynamical properties are considered. Indeed, despite a small increase in the variance, all the values are closer to the true ones. In particular, the Minimum-phase kernel, although able to retrieve asymmetries, fails to recover the good ratio between front and back slopes, both for crests and troughs. As said in previous sections, the symmetric kernel is unable to reproduce asymmetry in the records apart from vertical asymmetries. This is verified in the previous table and confirms

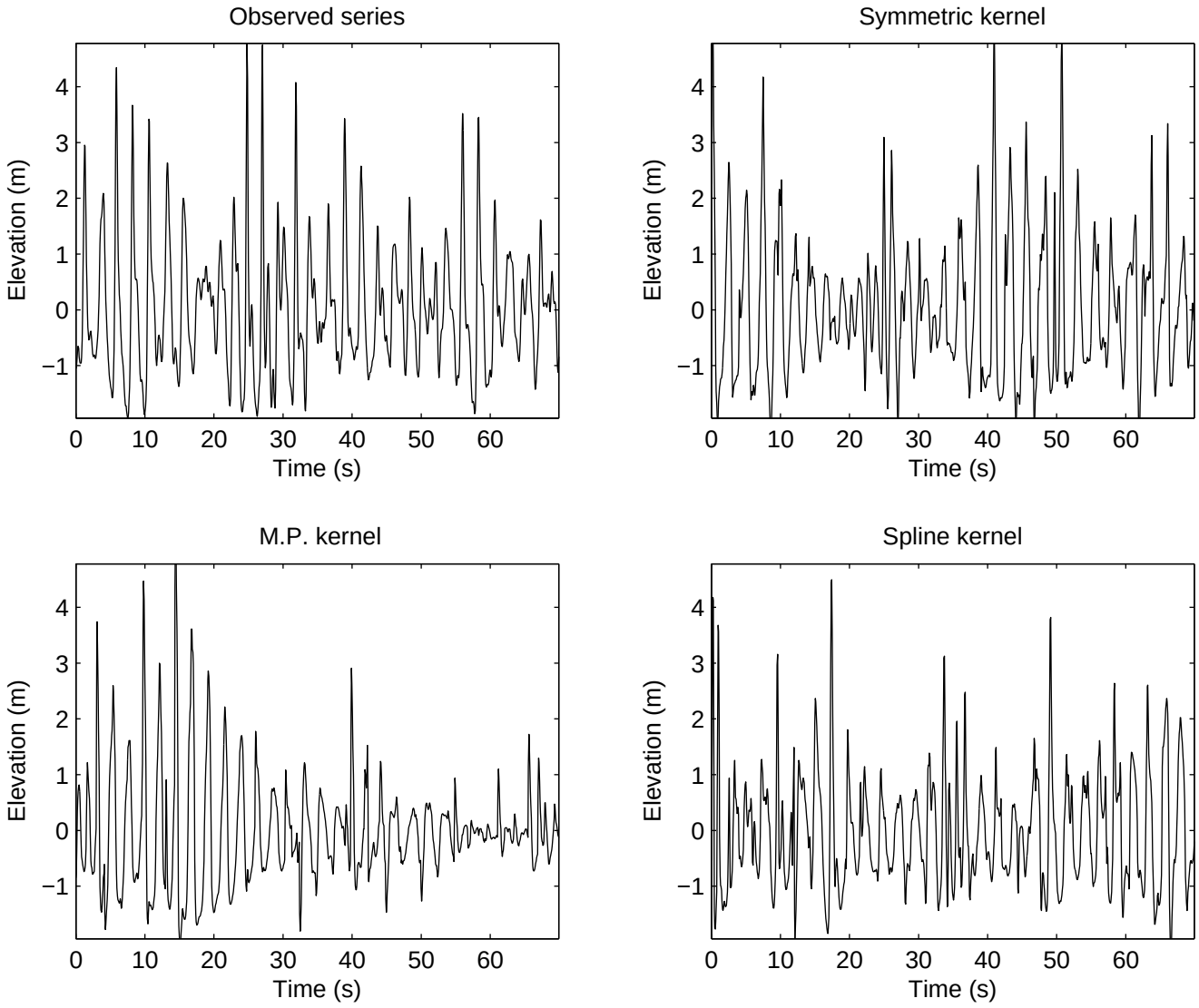

Figure 7: Example of trajectories of fitted processes.

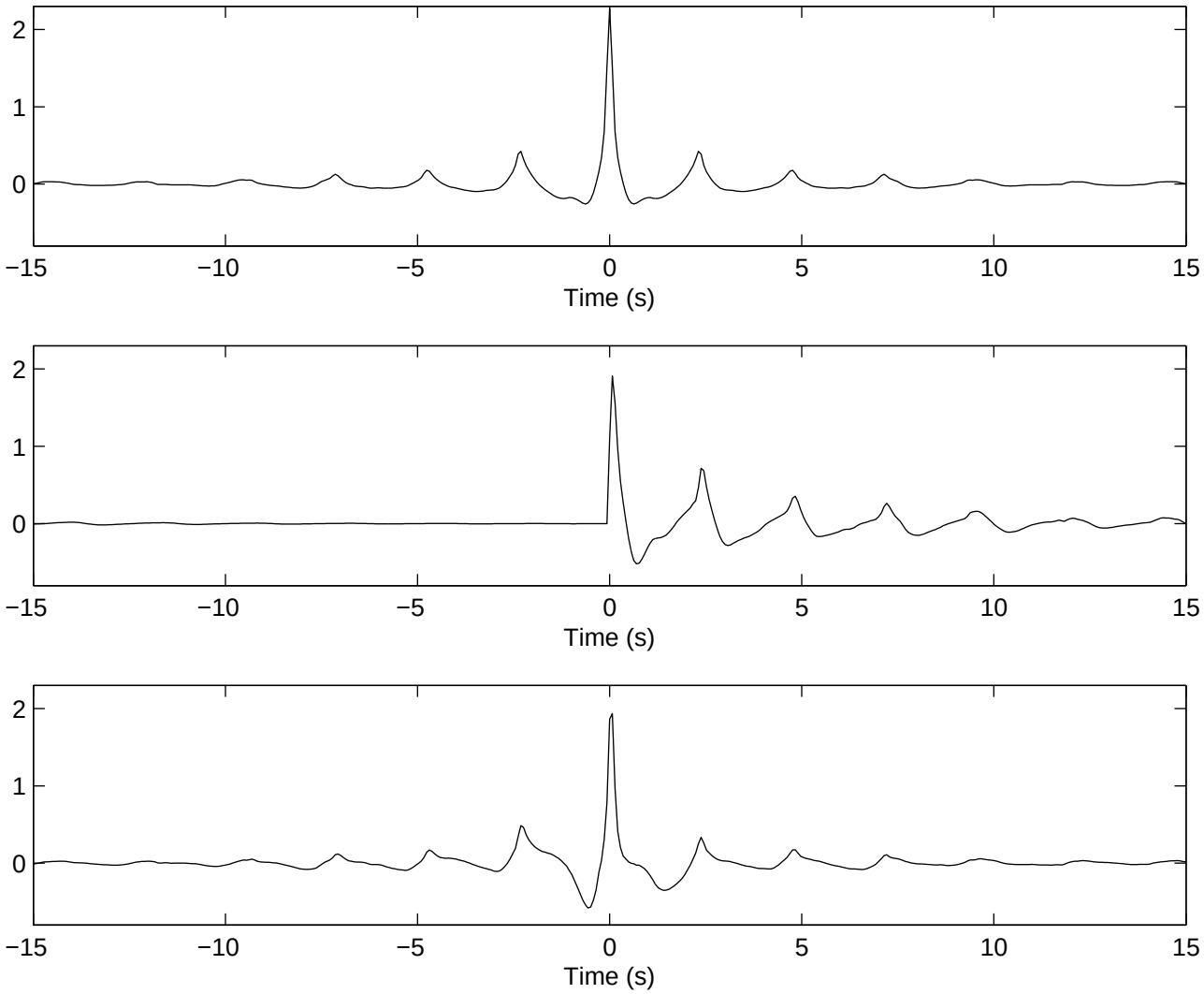

Figure 8: Estimated kernels. From top to bottom: symmetric model, minimum phase model, spline model.

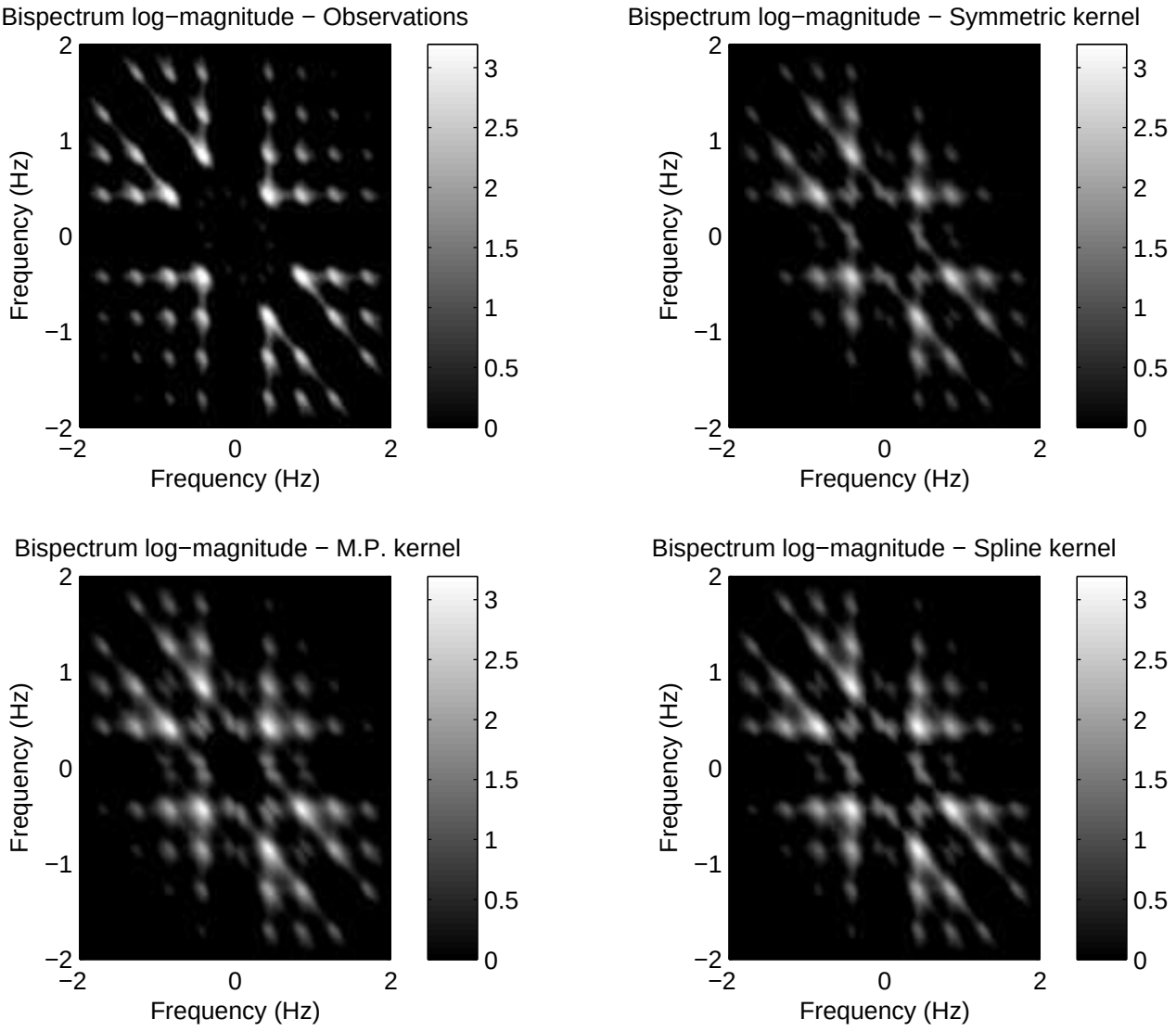

Figure 9: Log-magnitude of bispectra of observed process and fitted models.

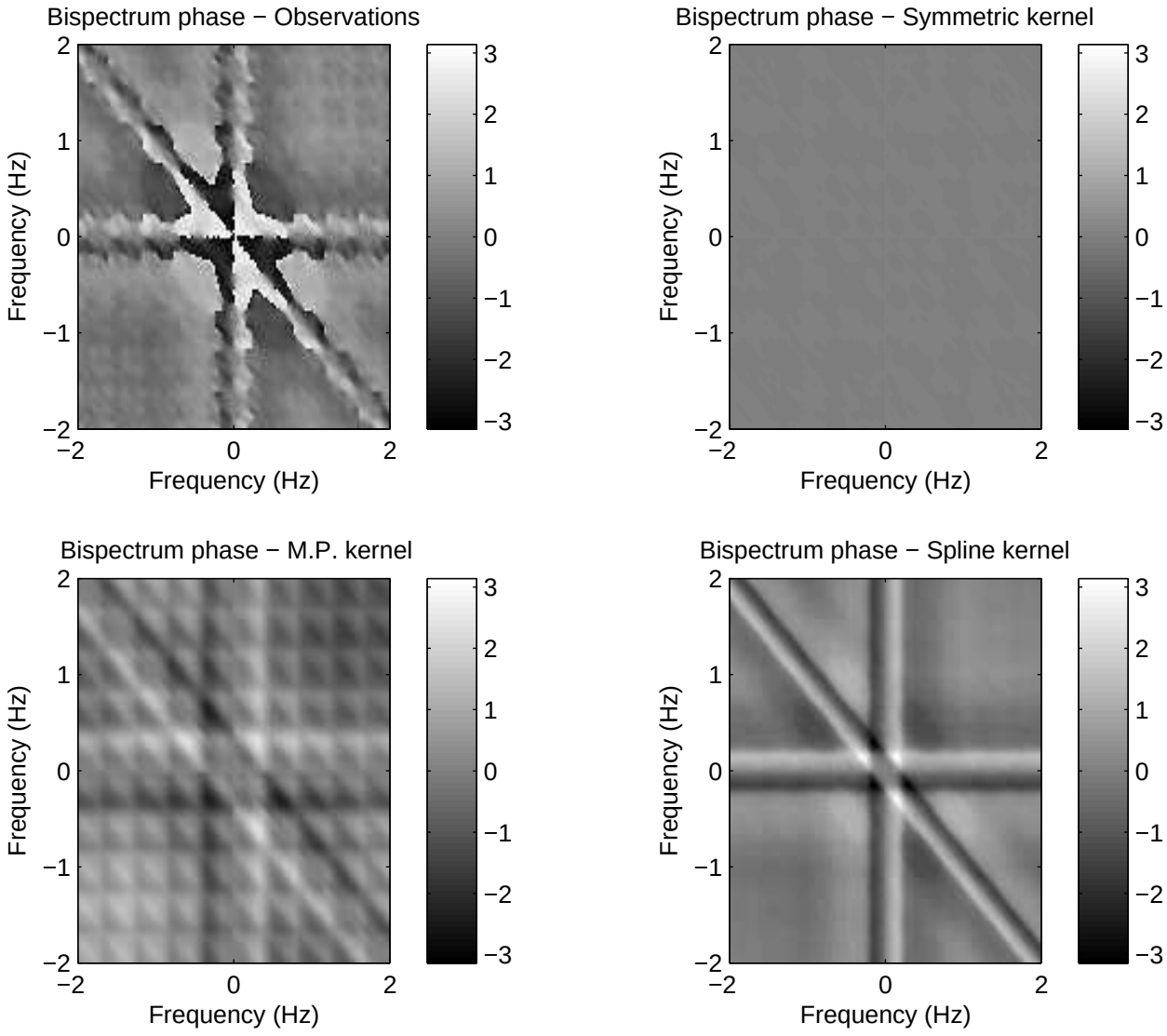

Figure 10: Angle of bispectra of observed process and fitted models.

that this type of kernel lacks flexibility to model non-linear time series.

Even if the Spline model is the closest one to the data, it still fails to catch the true values. This might be due to constraints due to linear filtering, since all of the complex features cannot be cough. To check this, we performed a linearity test based on the bicoherence (see [10]) which rejected the linearity of the process. Hence, the discrepancies between the fitted model and the observed data may be linked to the choice of a too restrictive model.

6. Conclusion

In this article we proposed a method to model time series that exhibits both horizontal and vertical asymmetries. The model is based on a novel versatile tool, called $\mathcal{LMA}$, which involves four parameters for the marginal distribution and a function called kernel. A new estimator based on splines has been proposed to estimate this function. Thanks to an inclusive numerical study, the performances of the new model have been checked and it shows great improvement compared to the previous estimator available. Some future work is also left on the construction of a parametric model on the phase of the transfer function to ease the estimation procedure.

We also tested the proposed methodology on a time series of sea waves. We checked that both horizontal and vertical asymmetries are well respected, along with dynamical parameters such as the skewness of the Hilbert transform or the crests and troughs slopes. The procedure shows great enhancement compared to existing methods concerning $\mathcal{LMA}$ but it still shows some discrepancies, that seems to come from the non-linearity of the data, which was found from a test based on the bispectrum. Hence, some improvements are still needed to overcome this, by using a second-order model to enhance the model.

Acknowledgements

The authors gratefully acknowledge the financial support from national French ANR project MODNAT.

References

1. Podgórski K, Wegener J. Non-gaussian fields with vertical and horizontal asymmetries. *Preprint* 2010;.

2. Aberg S, Podgórski K. A class of non-gaussian second order random fields. *Extremes* 2011;14:187–222. 10.1007/s10687-010-0119-1.

3. Galtier T, Gupta S, Rychlik I. Crossings of second-order response processes subjected to lma loadings. *J Probab Stat* 2010;2010:22 p. doi:10.1155/2010/752452.

4. Galtier T. Note on the estimation of crossing intensity for laplace moving average. *Extremes* 2011;14:157–66. 10.1007/s10687-010-0116-4.

5. Podgórski K, Wegener J. Estimation for stochastic models driven by laplace motion. *Communications in statistics Theory and methods* 2011;40.

6. Kotz S, Kozubowski T, Podgorski K. The Laplace Distribution and Generalizations: A Revisit With Applications to Communications, Exonomics, Engineering, and Finance. Progress in Mathematics Series; Birkhäuser Boston; 2001. ISBN 9780817641665.

7. Funke E, Mansard E. The control of wave asymmetries in random waves. *Coastal Engineering Proceedings* 1982;1(18).

8. Masuda A, Kuo YY. A note on the imaginary part of bispectra. *Deep Sea Research A* 1981;28:213–22. doi:10.1016/0198-0149(81)90063-7.

9. Elgar S. Bispectra of shoaling ocean surface gravity waves. In: *Higher-Order Spectral Analysis, 1989. Workshop on*. 1989:206–11. doi:10.1109/HOSA.1989.748765.

10. Nikias C, Petropulu A. Higher-order spectra analysis: a nonlinear signal processing framework. Prentice Hall signal processing series; PTR Prentice Hall; 1993. ISBN 9780136782100.

11. Rao TS, Gabr M. An introduction to bispectral analysis and bilinear time series models. Lecture Notes in Statistics, 24. New York etc.: Springer-Verlag. VIII, 280 p. DM 43.00; $ 15.10 (1984).; 1984.

12. Wegener J. Noise Convolution Models: Fluids in Stochastic Motion, Non-Gaussian Tempo-spatial Fields, and a Notion of Tilting. Doctoral theses in mathematical sciences; Faculty of Engineering, Centre for Mathematical Sciences, Mathematical Statistics, Lund University; 2010. ISBN 9789174730326.

13. Pan R, Nikias C. The complex cepstrum of higher order cumulants and nonminimum phase system identification. *Acoustics, Speech and Signal Processing, IEEE Transactions on* 1988;36(2):186–205. doi:10.1109/29.1513.

14. Fan J, Yao Q. Nonlinear Time Series: Nonparametric and Parametric Methods. Springer Series in Statistics; Springer; 2008. ISBN 9780387693958.

15. Cambanis S, Podgórski K, Weron A. Chaotic behavior of infinitely divisible processes. *Studia Mathematica* 1995;115(2):109–27.

16. Becq-Girard F, Forget P, Benoit M. Non-linear propagation of unidirectional wave fields over varying topography. *Coastal Engineering* 1999;38(2):91 – 113. doi:http://dx.doi.org/10.1016/S0378-3839(99)00043-5.

17. Hasselmann K, Barnett T, Bouws E, Carlson H, Cartwright D, Enke K, Ewing J, Gienapp H, Hasselmann D, Kruseman P, et al. Measurements of wind-wave growth and swell decay during the joint north sea wave project (jonswap). Tech. Rep.; Deutches Hydrographisches Institut; 1973.

18. Benton D, Krishnamoorthy K. performance of the parametric bootstrap method in small sample interval estimates. *Advances and Applications in Statistics* 2002;2.